2D Materials

PAPER

RECEIVED
5 September 2017

REVISED
1 February 2018

ACCEPTED FOR PUBLICATION
2 February 2018

PUBLISHED
20 February 2018

A new series of two-dimensional silicon crystals with versatile electronic properties

Kisung Chae[1], Duck Young Kim[2] and Young-Woo Son[1]

[1] Korea Institute for Advanced Study, Seoul 02455, Republic of Korea
[2] Center for High Pressure Science and Technology Advanced Research, Shanghai 201203, People's Republic of China

E-mail: hand@kias.re.kr

Keywords: first principles calculations, new silicon crystals, ab initio structure search method

Supplementary material for this article is available online

Abstract

Silicon (Si) is one of the most extensively studied materials owing to its significance to semiconductor science and technology. While efforts to find a new three-dimensional (3D) Si crystal with unusual properties have made some progress, its two-dimensional (2D) phases have not yet been explored as much. Here, based on a newly developed systematic *ab initio* materials searching strategy, we report a series of novel 2D Si crystals with unprecedented structural and electronic properties. The new structures exhibit perfectly planar outermost surface layers of a distorted hexagonal network with their thicknesses varying with the atomic arrangement inside. Dramatic changes in electronic properties ranging from semimetal to semiconducting with indirect energy gaps and even to one with direct energy gaps are realized by varying thickness as well as by surface oxidation. Our predicted 2D Si crystals with flat surfaces and tunable electronic properties will shed light on the development of silicon-based 2D electronics technology.

1. Introduction

Recently, various 2D materials with weak van der Waals (vdW) interlayer interaction have been extensively studied due to their unusual properties [1–3]. Examples of these include graphene, hexagonal boron nitride, black phosphorous, and transition metal dichalcogenides. Not only that they have shown superior physical and chemical properties, some of the models in theoretical physics such as massless Dirac fermions have also been realized in experiments, which otherwise have not been observed in conventional materials [1]. Nevertheless, many practical issues about large-scale synthesis, processing for defects, and contaminant control still need to be resolved [1, 4], which are critical for them to be realized as next generation electronic devices and energy applications.

Silicon, on the other hand, has served as a mainstay of semiconductor technologies, and a vast amount of advanced processing techniques have been accumulated for decades. It is mainly due to its abundance on the Earth surface as well as the existence of a single oxide form (SiO_2) which is advantageous to the mass production of a single-element device that is free from phase separations. These make undoubtedly Si be unique in current semiconductor technologies. Therefore, despite very active researches on the aforementioned 2D materials as a next generation platform for various applications, the best candidate may still be Si itself. This leads us to believe that discovering a novel 2D phase of Si materials with desirable physical properties would be important. Compared with the number of efforts for new bulk phase of Si [5–19], however, searching for a new 2D Si crystalline phase has not been remarkably succeeded yet, and only a few theoretical predictions [20–27] and experimental reports [28–33] exist in the literature.

Silicene [34–40], a monolayer form of the 2D Si crystals which is analogous to graphene, cannot form a stable layered structure by itself since surface of the silicene is chemically reactive, so that the adjacent silicene layers form strong covalent bonds [1, 37]. This is due to the strong preference of Si for the sp^3 hybridization over the sp^2 in contrast to carbon with the same number of valence electrons. Thus, silicene may not be a good candidate for a scalable 2D phase of Si [1]. In addition, due to the strong covalent bonding character of Si, as-cleaved surfaces inevitably have unpaired electrons localized at dangling bonds on the surface, which makes an energetically unfavorable situation. This is

evidenced by prevalent severe surface reconstruction to reduce the number of unpaired electrons as can be seen in most of the previously reported 2D Si crystals [21–27, 33]. In all the cases, however, some of the surface atoms still remain under-coordinated even after the reconstruction, implying that those atoms prone to form strong covalent bonding with one another as pointed out in the case of silicene [1, 37].

In this work, we theoretically predict a series of novel 2D allotrope of Si crystals constructed by a concrete *ab initio* materials search strategy. The predicted 2D crystals show characteristic structural features as follows. The crystal is composed of two parts: (1) the atomically flat surface layers and (2) the inner layer connecting them through sp^3-like covalent bonds as seen in figure 1. The surface layer features perfectly planar stable hexagonal framework unlike other 2D Si crystals that have hitherto been studied [21–33], in which buckled surfaces are predominant. Moreover, the crystal is completely free from coordination number (CN) defects. The structures composed of two parts are revealed stable against serious perturbations as will be discussed later.

2. Computational details

We concisely describe a novel 2D crystal structure prediction method: namely, Search by *Ab initio* Novel Design via Wyckoff position Iterations in the Conformational Hypersurface (abbreviated as SANDWICH), which explores the conformational hyperspace to find various local minima systematically. The method is especially suited for predicting 2D phases of covalent materials by designing the 2D crystals free of CN defects. This can be achieved by building surface and inner parts with different symmetries from each other, and by joining the two parts in such a way that under-coordinated atoms at the interface are compensated by one another. By doing so, the crystal becomes stabilized by eliminating dangling bonds.

Specifically, we chose surface layers to have a space group of P6/mmm (No. 191), while the bulk maintains a sp^3 bonding character. Among special positions in the given space group, we find that Wyckoff sites of *e* (0, 0, ±z) with a point group of 6 mm and i[(1/2, 0, ±z), (0, 1/2, ±z) and (1/2, 1/2, ±z)] with the group of 2 mm are suitable for building the CN defect-free crystals. Also, we considered two relative positions of the surface layers in this study, represented by displacement vectors of $\vec{d} = \mathbf{0}$ and $\vec{d} = 0.5\vec{a}_1 + 0.5\vec{a}_2$, where $\vec{a}_1$ and $\vec{a}_2$ are lattice vectors. With all the settings described so far, we generated structures by varying the number of atoms in the inner layer (n) consecutively from 0 up to 9. Our method exhausts all the possible combinations for atomic positions of 2D crystals with given constraints: surface symmetry, choice of Wyckoff positions and thickness as schematically shown in figure S1. We note that the method is undoubtedly advantageous since it explores almost all the structures from a highly probable subset of the entire search space for given conditions. More detailed descriptions of our SANDWICH method can be found in the supplementary data (stacks.iop.org/TDM/5/025013/mmedia).

We performed a series of first-principles calculations to obtain optimized structures by using Vienna *ab initio* simulation package (VASP) code [41, 42]. Conjugate gradient method was used to find the equilibrium structures with a force criterion of 1 meV $\mathring{A}^{-1}$. For Kohn–Sham orbital, core part was treated by using projector augmented wave method [43], while the valence part was approximated by linear expansion of a plane wave basis set with the kinetic energy cutoff of 450 eV. Self-consistent field of DFT was iterated until the differences of the total energy and eigenvalues are less than 10^{-7} eV. Numerical integration in the first Brillouin zone (BZ) was done on the Γ-centered $12 \times 12 \times 1$ grid meshes generated by a Monkhorst–Pack scheme. The exchange-correlation functional of Perdew–Burke–Ernzerhof was used to build the Hamiltonian of an electron–ion system [44]. For a better description of electronic structures with a band gap, a hybrid functional of Heyd–Scuseria–Ernzerhof [45] as implemented in the VASP code was used. Dynamical stability was also checked on each of the relaxed structures. Phonon dispersion spectra were generated by using a direct method [46] as implemented in phonopy package [47]. To obtain force constants, we used $4 \times 4 \times 1$ and $5 \times 5 \times 1$ supercells to generate displaced configurations. In this case, the k-point sampling in the BZ was done on the $24 \times 24 \times 1$ and $25 \times 25 \times 1$ Monkhorst–Pack grids.

3. Results and discussion

The 2D Si crystals constructed by the SANDWICH method demonstrate unique structural features. As we intentionally put together two symmetrically distinct parts (surface and inner layers) so that CN defects on both components are fully compensated by each other, all the atoms in the crystal have a CN of 4 without any dangling bonds as shown in figure 1(a). This condition is particularly favored for Si atoms which show strong preference for sp^3 bonding. We find that the four-coordinated networks are maintained in the fully relaxed equilibrium structures. Moreover, the crystals exhibit atomically flat surface structures without buckling or reconstruction, which is uncommon for 2D Si crystals except for silicene bilayers [21, 27]. Note that those bilayers with planar surfaces are nothing but the cases in our model with ($\vec{d} = \mathbf{0}$, $n = 0$) [21] and ($\vec{d} = 0.5\vec{a}_1 + 0.5\vec{a}_2, n = 0$) [27].

Looking into the structures in detail, we find that the surface and inner layers have different bonding characteristics as expected from the fact that they initially had different symmetries. The surface layers show distorted hexagonal lattices with additional bonds toward the inner layer, while the atoms in the

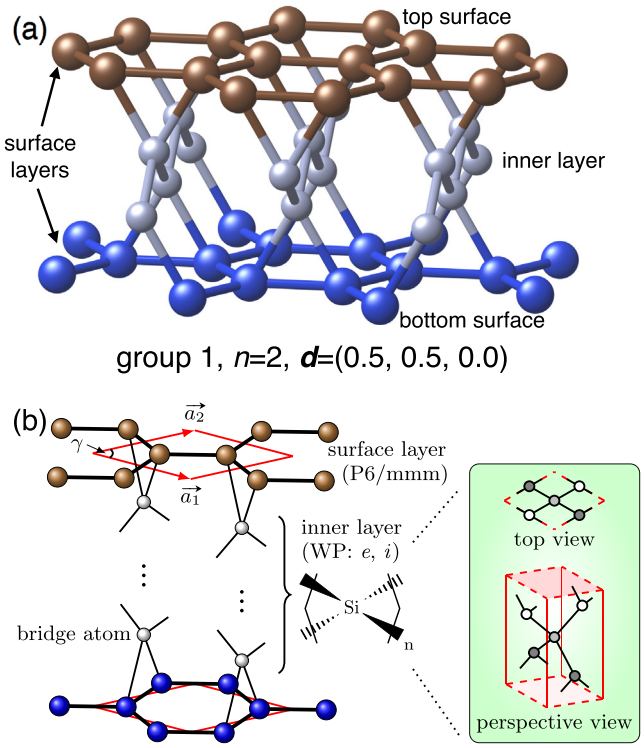

Figure 1. Atomic configuration of the 2D Si crystals. (a) A ball-stick model of the ground state geometry of a 2D Si crystal. Si atoms in top and bottom surface layers are shown in brown and blue balls, respectively, while those in the inner layer, sandwiched by the surface layers, are shown in gray balls. The displacement vector ($\vec{d}$) refers to the relative in-plane displacement of the two surface layers. (b) Schematic diagram of general 2D Si crystals. The unitcell is drawn in red with lattice parameters $\vec{a}_1$ and $\vec{a}_2$ marked. The inner layer is represented as a distorted tetrahedron, in which filled and dashed wedges by a Cram representation indicate bonds going out of and into the paper, respectively. Top and perspective views of the tetrahedrons in the inner layer are attached on aside, where the atoms in different layers are shaded differently using a gray gradient.

inner layer (hereafter called as bridge atoms as denoted in figure 1(b)) form distorted tetrahedral bonding with its two opposite edges parallel to the plane of the surface (figure 1). The atomic arrangement of the inner layer is similar to that of the {100} surfaces of the cubic diamond phase (dSi) distorted by an in-plane shear strain. We note that the key role of the outermost bridge atom located on the bond center of the surface atoms for stabilizing the characteristic planar surface structure of the crystals, which would not have been realized otherwise. Due to the discrepancy of the preferred local environments for the two parts in the common unitcell, some of the local structures must be distorted for compatibility. For instance, the angle between those bridge atoms and surface atoms is largely deviated from the ideal value of ~109.5 degrees (°) to ~60°. Also, the angles between the two skew lines (marked as thick dashed lines in figure 2(a)) are deviated from the right angle (90°) for some of the tetrahedrons made by bridge atoms, which creates torsional restoration forces as explained in figure 2(a). Among the unique structural features shared by the crystals in this study (namely, flat surfaces without CN defects), we find that a set of 2D crystals constructed with the same $\vec{d}$ and n display a variety of microstructures depending on the atomic arrangement in the inner layer. This comes from the various relative orientations of the distorted sp^3 bonds as explained above.

The global stress of the crystals is also affected critically by the $\vec{d}$, n and the atomic arrangement in the inner layer, making the unitcells distorted in various ways (table S1). Thus, for the sake of discussion, we classify the crystals into three distinct groups. (1) The crystals in the first group (group 1) are characterized by the same magnitudes of the lattice vectors ($|\vec{a}_1| = |\vec{a}_2|$) and reduced cell angle ($\gamma < 60°$). In this case, the unitcell is distorted by the normal components (σ_x and σ_y) only, as the shear component (τ_{xy}) is vanished due to symmetry as illustrated in figure 2(b). All the crystals in this group have $\vec{d} = 0.5\vec{a}_1 + 0.5\vec{a}_2$. Those crystals fall into the C222 space group, except for the case of $n = 2$ which is in the Cmme group as in the table S1. The magnitude of the global stress seems to be decreasing for thicker crystals (or with the increased n), indicated by the γ approaching to 60°. (2) The crystals in the second group (group 2) feature the symmetric lattice vectors ($|\vec{a}_1| = |\vec{a}_2|$) with $\gamma > 60°$. As in the case of group 1, only the σ_x and σ_y distort the unitcell without shear strain because of the symmetry; the crystals also fall into the space group of C222. Crystals in group 1 and 2 differ by the signs of the normal stresses as indicated in figure 2(b). The crystals in group 2 have two subgroups of $\vec{d} = \mathbf{0}$ and $\vec{d} = 0.5\vec{a}_1 + 0.5\vec{a}_2$. They behave differently in terms of the γ with respect to the n as can be seen in the table S1. In the former case, symmetry of the surface layers overtakes that of the inner

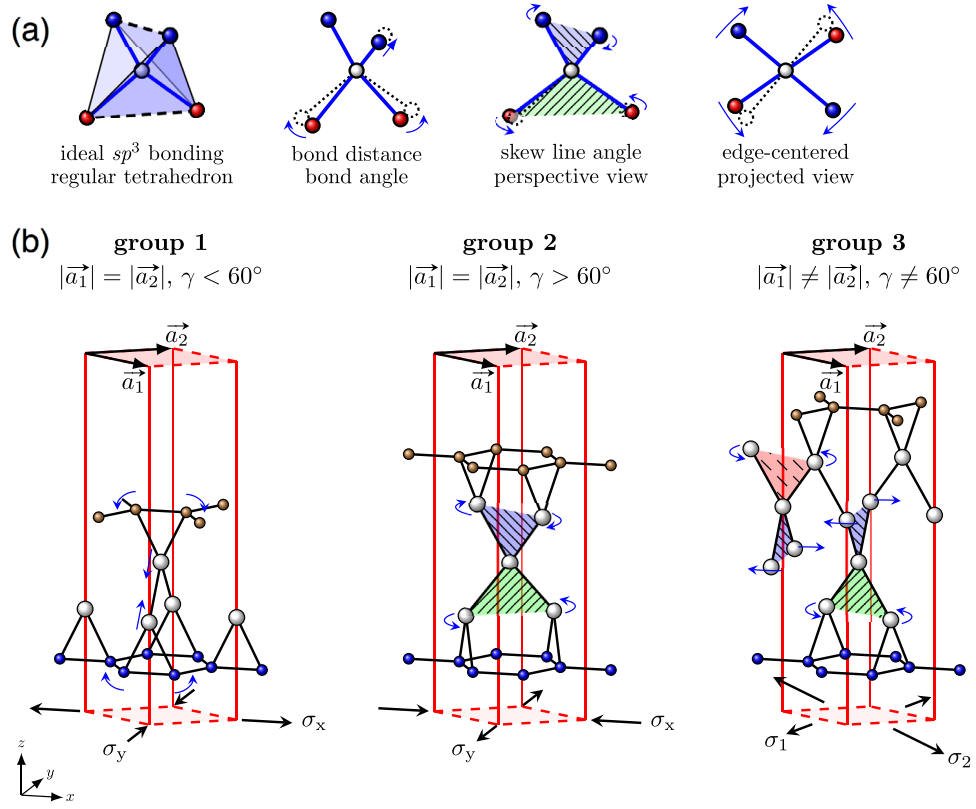

Figure 2. Classification of the 2D Si crystals. (a) Type of distortions in a tetrahedron building block. On the undistorted regular tetrahedron, skew lines along in-plane directions are marked as thick dashed lines. Bond stretch, bending, and twist are shown aside. The undistorted configurations are drawn in dotted lines for comparison, and restoration forces due to the distortion are shown in blue arrows. (b) Classification of the crystals due to various lattice distortions. Local and global stresses are shown in blue and black arrows, respectively. Group 1: local distortions in the surface layers mainly due to bond bending lead to the global stresses of positive (negative) normal stress along x (y) axis. Group 2: the unitcell is deformed by twist-like distortions in the inner layer, resulting in negative (positive) normal stress along x (y) axis. Group 3: dihedral angle distortions from different inner layers yield nonzero shear stress, so that the deformation of the unitcell becomes asymmetric ($|\vec{a}_1| \neq |\vec{a}_2|$).

layer, and the γ approaches to 60° as the n increases. On the other hand, the crystals with the $\vec{d} = 0.5\vec{a}_1 + 0.5\vec{a}_2$ subgroup are dominated by the symmetry of the inner layer, making the γ approach to 90° as the n increases. (3) Lastly, group 3 crystals are constructed with nonzero τ_{xy}, resulting in the asymmetric lattice vectors ($|\vec{a}_1| \neq |\vec{a}_2|$) as well as the space group of P2 with lower symmetry. In this case, the principal stresses (σ_1 and σ_2) do not agree with the σ_x and σ_y due to the τ_{xy}.

Stability of the crystals is confirmed as shown in figure 3. Cohesive energies (E_{coh}) for each crystal are plotted with respect to the number density, defined as the number of Si atoms in the unitcell divided by the unitcell area ($|\vec{a}_1 \times \vec{a}_2|$). In all the proposed cases, well-defined energy minima are shown as in figure 3(a). When compared with other Si structures, the crystals in this study show slightly higher E_{coh}. For example, with a number density of ~0.4 Si Å^{-2}, the crystal with a thickness of 0.5 nm shows a higher E_{coh} by 0.02 eV/atom than that of 2 × 1-dSi (1 0 0) with a thickness of 0.6 nm. We ascribe this to the significant distortion in bond angle especially near the surface as mentioned above. We note, however, that the 2D crystals in this study may stay more stable than other crystals in a chemical environment because the dangling bonds on the surface were eliminated. This chemical stability undoubtedly becomes a critical factor for device realization [1, 4]. Moreover, a recently synthesized allotrope of the 3D Si crystals, namely Si_{24}, also shows distorted bond angles ranging from 93.73° to 123.17°, and extended bond distances with a higher total energy than that of the ground state dSi by 0.09 eV/Si [11]. Thus, for realization of stable Si crystals, it could be more critical for the individual Si atoms to satisfy the ground state CN than to maintain the exact bond angles and distances of the ideal sp^3 bonding found in dSi. We also provide harmonic phonon dispersion spectra in figure 3(b) for the 2D crystals in the three groups. In all the cases, we confirm that the crystals are dynamically stable.

Furthermore, we find that the new 2D Si crystals are quite stable against strong perturbations beyond a usual harmonic interatomic force regime. To check such a structural stability, we generated computationally 'shaken' structures that have been proved useful to check the stabilities of other crystal structures [48] (see supplementary data). Starting from the fully relaxed crystal in group 1 with $n = 2$, we displaced every Si atom in a random direction with a fixed amount of 0.5 Å, in the 2 × 2 supercell. Note that we used the significantly large displacement when compared with that of 0.01 Å, used to obtain harmonic interatomic force constants (figure 3(b)).

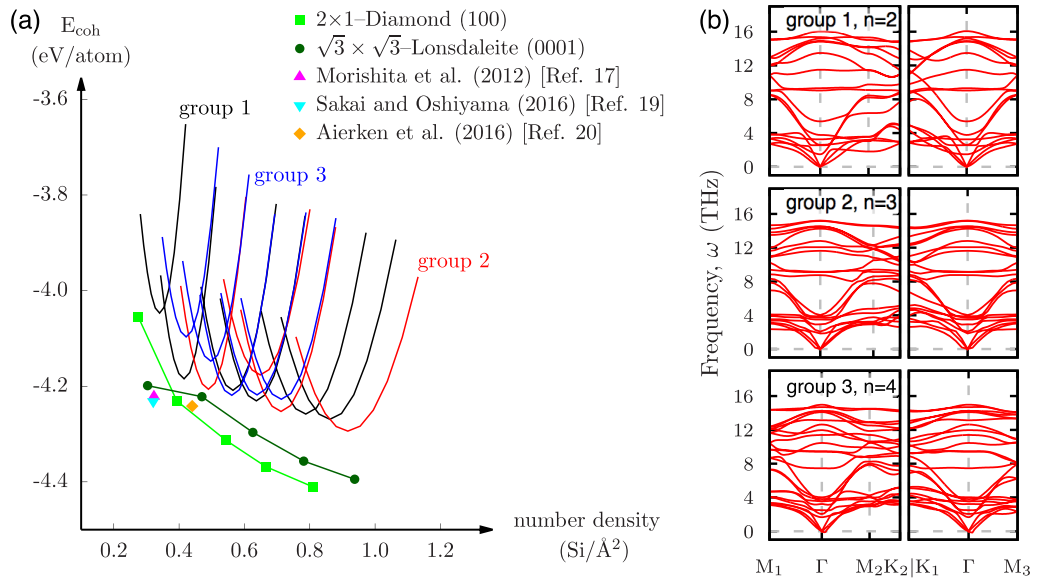

Figure 3. Stability of the crystals. (a) Cohesive energy (E_{coh}) of the 2D crystals with respect to the number density. (b) Harmonic phonon dispersion spectra for a representative structure in each group.

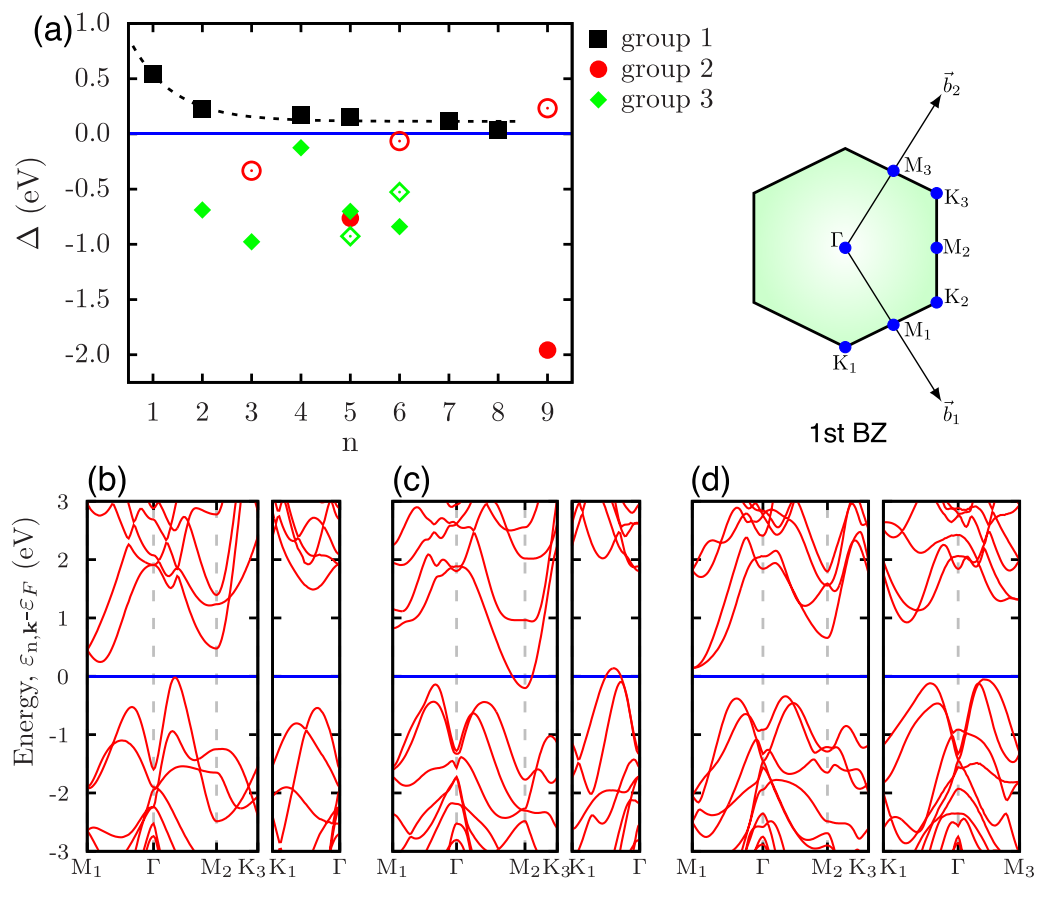

Figure 4. Electronic structures of the 2D crystals. (a) Bandgap (Δ) as a function of thickness (n) is shown for the 2D crystals in each group. In group 2 and 3, empty and filled symbols indicate the displacement vectors $\vec{d} = \mathbf{0}$ and $\vec{d} = 0.5\,\vec{a}_1 + 0.5\,\vec{a}_2$. Electronic band dispersion of (b) group 1 with $n = 2$, (c) group 2 with $n = 3$ and (d) group 3 with $n = 4$. A schematic diagram of the 1st BZ with high symmetry points is shown above (d).

Then, each of the perturbed structures was relaxed to the corresponding energy minimum configurations by using the conjugate gradient method. By comparing ~5500 randomly generated configurations, we found that our proposed structure was retained in the ~3500 samples after relaxation, proving that the structure is robust against severe thermal fluctuations as shown in the figure S2.

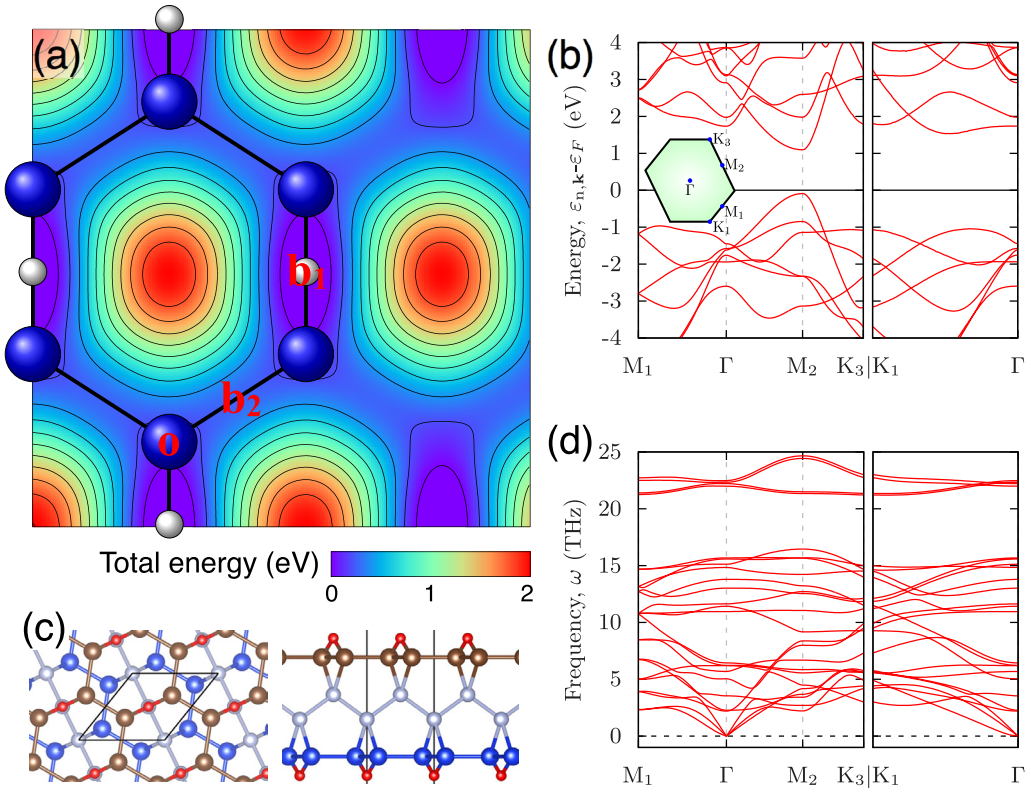

Figure 5. Oxidation of the 2D Si crystal. (a) Potential energy surface of the 2D crystal by an O probe atom with a height of 2 Å. Atoms are superimposed on the map: large blue and small white balls indicate surface silicon atoms and underneath bridge silicon atoms, respectively. The minimum energy for adsorption site at b_1 is set to be zero in the color bar shown below. (b) Electronic band dispersion and (c) atomic structure of the fully oxidized crystal in ground state. Adsorbed oxygen atoms are denoted by small red balls. (d) Phonon dispersion spectra of the oxidized 2D Si crystal is also shown.

The fundamental electronic structures of the crystals are closely related to their thickness (n) and the crystal classification defined above, displaying a wide variety of electronic properties ranging from metallic to semiconducting. For instance, all the crystals categorized as group 1 are semiconductors, showing a finite bandgap ($\Delta > 0$) with their sizes decreasing with an increasing n as shown in figure 4(a). The maximum size of the energy gap is ~0.5 eV for the thinnest crystal ($n = 1$). On the other hand, most of the crystals in group 2 and group 3 are metallic. Note that the Δ in this case is a measure of the overlap between the conduction and valence energy bands. For group 2, the Δ behaves differently with respect to the n depending on the subgroup ($\vec{d}$) as discussed above.

To reveal the origin of various electronic phases in the crystal families, we provide electronic band dispersions for each group in figures 4(b)–(d). Edges of the valence and the conduction bands are located at different momenta ($\vec{k}$), indicating that the crystals are either indirect semiconductors or semimetals. For the crystals with a space group of C222 (group 1 and 2), we note that the relative energetic positions of the bands at $\vec{k} = 0.5\vec{b}_1$ (ϵ_{M_1}) and $\vec{k} = 0.5\vec{b}_1 + 0.5\vec{b}_2$ (ϵ_{M_2}) are directly responsible for the electronic phase transition. Here, $\vec{b}_1$ and $\vec{b}_2$ indicate the reciprocal lattice vectors in the BZ as shown in figure 4. That is to say, when the conduction band minimum (CBM) is located at M_1, the crystals represent finite energy gaps ($\Delta > 0$), while semimetallic phases with $\Delta < 0$ are realized for crystals with the CBM located at M_2 as seen in figures 4(b) and (c). Note that the crystals in group 1 and 2 belong to the former and the latter cases, respectively. Because crystals are classified by the lattice parameters of the unitcell (figure 2), we ascribe the electronic phase transition to the changes in the local atomic structures due to the lattice parameters, especially to the γ. We firstly confirm that the electronic wave functions for the CBM are highly localized near the surface layers (figure S3), indicating that the surface geometry is mainly responsible for the electronic phase transition. We further verify this by pure shear deformation of the unitcell only to change the γ without changing $|\vec{a}_1|$ and $|\vec{a}_2|$, and see that the crossover between ϵ_{M_1} and ϵ_{M_2} indeed occurs as shown in figure S4. Based on those facts, we can construct a concise but essential model for the whole crystal explaining the characteristic variation of electronic structures from semiconductor to semimetal as functions of thickness and group classification (see figure S5). In addition, these crystals provide good transport properties when compared to the dSi. We note that the transverse effective masses for electrons near the CBM are reduced by half when compared with the dSi, while similar values of other

components are shown as in the table S2. The structures with lower crystal symmetry (group 3) always show semimetallic electronic structures (figure 4(d)).

Interestingly, we find that the surface oxidation can extremely widen the applicability of the new crystals. With the oxygen (O) adsorption on the surface, the crystal in group 1 with $n = 2$ is significantly stabilized by 1.98 eV/O_2, and with the subsequent dissociation of the adsorbed O_2 molecule on the surface, the system becomes even more stabilized by 5.89 eV/O_2 (See supplementary data for details). We confirm that adsorption and dissociation of O_2 molecules do not affect much on the characteristic planar structure of the surface in a wide range of O coverage from an isolated limit (figure S8) to the full coverage (figure 5(c)). We find that the ground state occurs when the adsorbed O atom is located on the middle of the surface Si–Si bond just on top of the underneath bridge Si atom marked as b_1 in figure 5(a). Moreover, electronic properties vary notably via surface oxidation from the indirect energy gap of ∼0.2 eV (figure 4(a)) to the direct bandgap of ∼1.2 eV (Figure 5(b)), and the transverse effective masses for electron and hole are further reduced from 0.16 m_0 to 0.11 m_0 and from 0.19 m_0 to 0.13 m_0, respectively. This insulating behavior will significantly widen the versatility of the 2D Si crystals in this study including many electronic device applications, e.g. a metal-insulator switching device [49].

Finally, we discuss a possible synthesis mechanism of the oxidized 2D Si crystal. Owing to the severe distortion of the bond angle as discussed above, there would be a significant kinetic energy barrier for phase transition from a known structure, and processing parameters (e.g. doping, strain, temperature, etc) might not be accessible in experiment. Instead, we suggest that the oxidized 2D Si crystal could be synthesized by self-assembly of Si_3O cluster [50]. The Si_3O cluster forms a triangular Si network with the O atom bound with two Si atoms, and the bond angle between the Si atoms are ∼60°. Thus, high kinetic energy barrier expected for phase transition can be circumvented. We further confirm that the oxidized 2D crystals can form stable layered structure by itself, which also suggests that this Si material as a feasible candidate for a component in vdW heterojunction [1].

4. Conclusions

In this work, using a newly developed *ab initio* computational method, we propose a series of two-dimensional silicon crystals with versatile electronic properties. The surface layer of the new 2D Si crystals exhibits atomically flat distorted hexagonal structure without buckling, and the inner layer silicon atoms fill up the space between the flat surface layers. We classified 2D Si structures into three groups and each of the groups possesses distinct electronic properties originated from structural variations such as semiconductor as well as semimetals. Moreover, their oxidized forms are shown to be a direct bandgap semiconductor. Therefore, we believe that our new 2D Si crystals satisfy highly desirable characteristics of next generation electronic technology platforms only with a single atomic element and their oxides, very similar with the current 3D Si electronic devices.

Acknowledgments

The authors thank Dr In-Ho Lee for discussions. DYK acknowledges the support by the National Natural Science Foundation of China (Grant No. 11774015 and U1530402) and KIAS visitor supporting program. Y-WS was supported by the NRF of Korea funded by the MSIP (vdWMRC, No. 2017R1A5A1014862). The computing resources were supported by the Center for Advanced Computation of KIAS.

ORCID iDs

Kisung Chae https://orcid.org/0000-0003-1628-408X

References

[1] Geim A K and Grigorieva I V 2013 *Nature* **499** 419
[2] Novoselov K S, Jiang D, Schedin F, Booth T J, Khotkevich V V, Morozov S V and Geim A K 2005 *Proc. Natl Acad. Sci.* **102** 10451
[3] Lee C H *et al* 2014 *Nat. Nanotechnol.* **9** 676
[4] Lin Z, Carvalho B R, Kahn E, Lv R, Rao R, Terrones H, Pimenta M A and Terrones M 2016 *2D Mater.* **3** 022002
[5] Wentorf R H and Kasper J S 1963 *Science* **139** 338
[6] Kasper J S, Hagenmuller P, Pouchard M and Cros C 1965 *Science* **150** 1713
[7] Besson J M, Mokhtari E H, Gonzalez J and Weill G 1987 *Phys. Rev. Lett.* **59** 473
[8] Von Schnering H G, Schwarz M and Nesper R 1988 *J. Less-Common Met.* **137** 297
[9] Gryko J, McMillan P F, Marzke R F, Ramachandran G K, Patton D, Deb S K and Sankey O F 2000 *Phys. Rev.* B **62** R7707
[10] Malone B D, Sau J D and Cohen M L 2008 *Phys. Rev.* B **78** 035210
[11] Kim D Y, Stefanoski S, Kurakevych O O and Strobel T A 2015 *Nat. Mater.* **14** 169
[12] Rapp L, Haberl B, Pickard C, Bradby J, Gamaly E, Williams J and Rode A 2015 *Nat. Commun.* **6** 7555
[13] Botti S, Flores-Livas J A, Amsler M, Goedecker S and Marques M A L 2012 *Phys. Rev.* B **86** 121204
[14] Wang Q, Xu B, Sun J, Liu H, Zhao Z, Yu D, Fan C and He J 2014 *J. Am. Chem. Soc.* **136** 9826
[15] Lee I H, Lee J, Oh Y J, Kim S and Chang K J 2014 *Phys. Rev.* B **90** 115209
[16] Lee I H, Oh Y J, Kim S, Lee J and Chang K 2016 *Comput. Phys. Commun.* **203** 110
[17] Guo Y, Wang Q, Kawazoe Y and Jena P 2015 *Sci. Rep.* **5** 14342
[18] Luo K *et al* 2016 *Chem. Mater.* **28** 6441
[19] Liu Y, Jiang X, Huang Y, Zhou S and Zhao J 2017 *J. Appl. Phys.* **121** 085107
[20] Morishita T, Nishio K and Mikami M 2008 *Phys. Rev.* B **77** 081401
[21] Bai J, Tanaka H and Zeng X C 2010 *Nano Res.* **3** 694
[22] Morishita T, Russo S P, Snook I K, Spencer M J S, Nishio K and Mikami M 2010 *Phys. Rev.* B **82** 045419
[23] Morishita T, Spencer M J S, Russo S P, Snook I K and Mikami M 2011 *Chem. Phys. Lett.* **506** 221
[24] Spencer M J S, Morishita T and Snook I K 2012 *Nanoscale* **4** 2906

[25] Guo Z X, Zhang Y Y, Xiang H, Gong X G and Oshiyama A 2015 *Phys. Rev.* B **92** 201413
[26] Sakai Y and Oshiyama A 2015 *Phys. Rev.* B **91** 201405
[27] Aierken Y, Leenaerts O and Peeters F M 2016 *Phys. Chem. Chem. Phys.* **18** 18486
[28] Nakano H, Ishii M and Nakamura H 2005 *Chem. Commun.* **2005** 2945
[29] Nakano H, Mitsuoka T, Harada M, Horibuchi K, Nozaki H, Takahashi N, Nonaka T, Seno Y and Nakamura H 2006 *Angew. Chem. Int. Ed.* **45** 6303
[30] Kim U, Kim I, Park Y, Lee K Y, Yim S Y, Park J G, Ahn H G, Park S H and Choi H J 2011 *ACS Nano* **5** 2176
[31] Lu Z, Zhu J, Sim D, Zhou W, Shi W, Hng H H and Yan Q 2011 *Chem. Mater.* **23** 5293
[32] Kim W S, Hwa Y, Shin J H, Yang M, Sohn H J and Hong S H 2014 *Nanoscale* **6** 4297
[33] Ohsuna T, Morishita T, Hayasaka Y, Spencer M J S, Yaokawa R and Nakano H 2016 *Nat. Commun.* **7** 10657
[34] Takeda K and Shiraishi K 1994 *Phys. Rev.* B **50** 14916
[35] Guzmn-Verri G G and Lew Yan Voon L C 2007 *Phys. Rev.* B **76** 075131
[36] Cahangirov S, Topsakal M, Aktk E, Ahin H and Ciraci S 2009 *Phys. Rev. Lett.* **102** 236804
[37] Vogt P, De Padova P, Quaresima C, Avila J, Frantzeskakis E, Asensio M C, Resta A, Ealet B and Le Lay G 2012 *Phys. Rev. Lett.* **108** 155501
[38] Tao L, Cinquanta E, Chiappe D, Grazianetti C, Fanciulli M, Dubey M, Molle A and Akinwande D 2015 *Nat. Nanotechnol.* **10** 227
[39] Le Lay G 2015 *Nat. Nanotechnol.* **10** 202
[40] Grazianetti C I 2016 *2D Mater.* **3** 012001
[41] Kresse G and Furthmüller J 1996 *Phys. Rev.* B **54** 11169
[42] Kresse G and Furthmüller J 1996 *Comput. Mater. Sci.* **6** 15
[43] Kresse G and Joubert D 1999 *Phys. Rev.* B **59** 1758
[44] Perdew J P, Burke K and Ernzerhof M 1996 *Phys. Rev. Lett.* **77** 3865
[45] Krukau A V, Vydrov O A, Izmaylov A F and Scuseria G E 2006 *J. Chem. Phys.* **125** 224106
[46] Parlinski K, Li Z Q and Kawazoe Y 1997 *Phys. Rev. Lett.* **78** 4063
[47] Togo A and Tanaka I 2015 *Scr. Mater.* **108** 1
[48] Pickard C J and Needs R J 2011 *J. Phys.: Condens. Matter* **23** 053201
[49] Fiori G, Bonaccorso F, Iannaccone G, Palacios T, Neumaier D, Seabaugh A, Banerjee S K and Colombo L 2014 *Nat. Nanotechnol.* **9** 768
[50] Wang L S, Nicholas J B, Dupuis M, Wu H and Colson S D 1997 *Phys. Rev. Lett.* **78** 4450